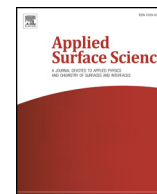


# ULRR

## Nanoscale topography, surface charge variation and defect correlation in 2–8 nm thick functional alumina films

Item Type	Article
Authors	Guinane, Luke;Gautam, Devendraprakash;Kubik, Jan;Stenson, Bernard;Geary, Shane;Lebedev, Vasily A.;Laffir, Fathima R.;Beloshapkin, Sergey;Ul Haq, Ehtsham;Tofail, Syed A.M.
Citation	Applied Surface Science;528, 146950
Publisher	Elsevier
Download date	2026-03-17 15:51:08
Item License	<a href="https://creativecommons.org/licenses/by-nc-sa/1.0/">https://creativecommons.org/licenses/by-nc-sa/1.0/</a>
Link to Item	<a href="https://hdl.handle.net/10344/8979">https://hdl.handle.net/10344/8979</a>



## Full Length Article

## Nanoscale topography, surface charge variation and defect correlation in 2–8 nm thick functional alumina films

Luke Guinane<sup>a,\*</sup>, Devendraprakash Gautam<sup>b</sup>, Jan Kubik<sup>b</sup>, Bernard Stenson<sup>b</sup>, Shane Geary<sup>b</sup>, Vasily Lebedev<sup>a</sup>, Fathima Laffir<sup>a</sup>, Sergey Beloshapkin<sup>a</sup>, Ehtsham Ul-Haq<sup>a</sup>, Syed A.M. Tofail<sup>a,\*</sup>

<sup>a</sup> Bernal Institute, University of Limerick, Limerick, Ireland

<sup>b</sup> Analog Devices International, Raheen Business Park, Limerick, Ireland

## ARTICLE INFO

## Keywords:

Al<sub>2</sub>O<sub>3</sub>  
Nanoscale  
RF magnetron sputtering  
KPFM  
Defects

## ABSTRACT

In the nanometric regime, alumina films are often deposited by ALD methods yet in industrial applications, sputtered films thinner than 40 nm are used and research into those is sparse. Here, we investigated the nanoscale topography and the electrical properties of films less than 10 nm thick deposited by direct RF magnetron sputtering. Alumina films deposited on Si appeared to be uniform and topographically defect free as evaluated by TEM and AFM. However, their composition varied as a function of thickness as measured by XPS. The films were non-stoichiometric as Al content increased with film thickness. While SSRM measured current profiles did not highlight leakage sites or voids in the films, KPFM measured local charge fluctuations across the films deposited on Si and Au surfaces. The density of fluctuation sites decreased with an increase of alumina thickness. An electrodeposition method identified insulation weak spots in the alumina where Cu growths formed on the alumina surface. The growth mechanisms were investigated by TEM and EDX. The density of growths decreased with increased alumina thickness. Defects in the deposited alumina film are expected to be due to its non-stoichiometric nature causing charge variations, which weaken the films electrical insulating capability.

## 1. Introduction

Alumina (Al<sub>2</sub>O<sub>3</sub>) is a material used as a functional layer in a range of CMOS and micro/nano-electromechanical system (M/NEMS) applications. Its large band gap and moderate dielectric constant [1] are desirable for use in gate dielectrics [2], capacitors [3] and memories [4]. Thin film alumina's high transparency [5] is useful for solar cells [6–8]. Additionally, its mechanical [9] and thermal stability [10] are useful for protective coatings [11]. As films enter the nanometric regime, their properties may be subject to change. Deposited thin films of Al<sub>2</sub>O<sub>3</sub> are usually amorphous (a-Al<sub>2</sub>O<sub>3</sub>) but due to substrate condition and processing effects, they have been reported to crystallise into alpha (α), delta (δ), eta (η), gamma (γ) and theta (θ) phases [12] affecting resistive, optical, thermal and mechanical properties [10].

The method of deposition will also impact the properties of Al<sub>2</sub>O<sub>3</sub>. Industry utilizes both chemical vapour deposition (CVD) and physical vapour deposition (PVD) methods. A CVD process commonly used in the solar cell industry is the atomic layer deposition (ALD) and extensions to this process [13]. The advantages of ALD include precise thickness control, film uniformity in high aspect ratio structures and high surface quality in ultra-thin films less than 10 nm [14]. The main

disadvantage of ALD is that it is a relatively slow and expensive process in film deposition when high throughput is required. Sputtering is a PVD technique used to deposit moderately thick films. There are several extensions to this process including radio frequency (RF) [6,15], pulsed DC [16], reactive [17] and direct [2] methods. Sputtering is a desirable technique from an industry perspective as it is a relatively quick and therefore cheap deposition technique for thin films. However, a significant drawback is that sputtering is a challenging technique for the deposition of ultra-thin films due to different growth mechanisms. This may increase nucleation spots and columnar grain growth [15], leading to pinhole formation and other defects in the film.

Although Al<sub>2</sub>O<sub>3</sub> is considered an improvement to standard silica (SiO<sub>2</sub>) in ultra-thin electronic applications, it is still subject to electrical leakage and other defects [18]. Identification, evaluation and ultimately removal of defects in ultra-thin Al<sub>2</sub>O<sub>3</sub> is required to optimise their performance as functional layers in different applications. Capacitance-voltage and current-voltage measurements are common macroscopic techniques used to investigate the electrical properties of the films. Such measurements inform the electrical state of the film and are sensitive to defects that affect the electrical state. These electrical techniques are better suited for device-level measurements as they test

\* Corresponding authors.

E-mail addresses: [luke.guinane@ul.ie](mailto:luke.guinane@ul.ie) (L. Guinane), [Tofail.syed@ul.ie](mailto:Tofail.syed@ul.ie) (S.A.M. Tofail).

<https://doi.org/10.1016/j.apsusc.2020.146950>

Received 20 March 2020; Received in revised form 5 June 2020; Accepted 9 June 2020

Available online 14 June 2020

0169-4332/© 2020 The Authors. Published by Elsevier B.V. This is an open access article under the CC BY license (<http://creativecommons.org/licenses/by/4.0/>).

much larger areas, in doing so, these large area measurements average out localised nanoscale electrical information [4]. As film thickness is reduced, electron traps and other defects tend to form, which will degrade the layer functionality and ultimately the device performance. Nanoscopic techniques including Atomic Force Microscopy (AFM), Kelvin Probe Force Microscopy (KPFM) and Scanning Spreading Resistance Microscopy (SSRM) are used to measure the surface state and electrical properties of thin films. KPFM in particular, is a beneficial technique for the analysis of charge trapped in the insulating thin films. Electrodeposition (ED) has been employed recently as a possible way to evaluate defects in ultra-thin films including composition, topography and thickness that correlates to a change in electrical properties such as conductivity. As the thickness of a film decreases to the nanometre scale, the number of structural defects can increase. This makes the retention of good insulating properties in such thin film a big challenge. The problem becomes more acute when ultrathin films are deposited on large production scale substrates as uniformity of film density and thickness become an issue in manufacturing process. Studies in literature on such ultra-thin  $\text{Al}_2\text{O}_3$  films are generally performed on relatively small substrates e.g.  $3 \times 3 \text{ cm}^2$  [2,3,10,12,13]. The challenge in controlling defects and maintaining good insulating properties is increased as the substrate areas become larger. This is in particular is a challenge for industrial scale processing where substrates may be up to 300 mm in diameter [15].

In this article, we investigated the correlation between the composition, surface topography, and the electrical properties of ultra-thin  $\text{Al}_2\text{O}_3$  films deposited on 200 mm diameter substrates by direct RF magnetron sputtering. We attribute thickness dependent changes in the alumina's composition to the fluctuation in the films surface potential distribution. The fluctuations are associated with the defect sites in the film contributing to insulation weak spots, that allows copper (Cu) to grow on the surface during electrodeposition. Our study provides a basis to identify defects in ultra-thin insulating films on large 200 mm diameter, industrial scale substrates. It provides a pathway to optimize RF sputter deposition parameters to improve the functionality of investigated films for CMOS, MEMS and NEMS applications.

## 2. Materials and methods

In the present investigation two sets of substrates were used. The first set consists of  $\langle 1\ 0\ 0 \rangle$  oriented silicon (Si) wafers, 200 mm in diameter. The Si surfaces were polished to provide a smooth surface as per semiconductor industry processing standards. The second set of wafers were processed such that the surface of the substrate was conductive prior to alumina deposition. For this second set, a 200 nm  $\text{SiO}_2$  layer was thermally grown on the Si wafer. Next, a conductive bilayer of gold and titanium tungsten (Au/TiW) were sputter deposited on the  $\text{SiO}_2$  surface without a vacuum break. The Au and TiW layers were 70 and 150 nm, respectively. The alumina films under investigation were deposited by direct RF magnetron sputtering from a stoichiometric  $\text{Al}_2\text{O}_3$  target. The target had dimensions of  $40 \text{ cm} \times 14.6 \text{ cm} \times 1.5 \text{ cm}$ . The system had a base pressure of  $10^{-6}$  mbar, 2.5 kW power and argon flow rate of 2.5 sccm. The deposition took place in a multi-material industrial deposition tool. The wafers were placed on a rotating drum that repeatedly passed the  $\text{Al}_2\text{O}_3$  target. The thickness of the film was controlled by the number of times the wafer passed the target and the rotation speed of the drum. The films deposited on the conductive surface were further processed. They were covered in a photoresist that was exposed and developed. Next, alumina not covered by the photoresist was wet etched away. Finally, the remaining photoresist was removed. (A classification of the substrates used, and their subsequent experiments are summarised in the [Supplementary information S.1](#))

Deposition rate was determined by measuring the deposited film thickness on the Si substrates using a JEOL 2100F, Transmission Electron Microscope (TEM). Cross-sectional samples were prepared by a FEI Helios G4 CX Dual Beam Focus Ion Beam (FIB) with a gallium ion

source. Electron diffraction mode in the TEM determined the structure of deposited film. The surface stoichiometry of these films was investigated by a Kratos AXIS Ultra X-ray Photoelectron Spectrometer (XPS). XPS was operated with a beam voltage of 15 kV and a beam current of 10 mA. The analysis area and depth of analysis were approximately  $1 \text{ mm}^2$  and 10 nm respectively. First, a survey spectrum was recorded, then followed by a high-resolution spectrum. Construction and peak fitting of synthetic peaks in narrow region spectra used a Shirley type background and the synthetic peaks were of a mixed Gaussian-Lorentzian type. Relative sensitivity factors used are from CasaXPS library containing Scofield cross-sections.

Surface topography and nanoscale electrical properties were measured using NT-MDT's Ntegra Spectra II, a multi-modal scanning probe microscope (SPM). Topography was recorded using semi-contact AFM. Current profiles and subsequent local material resistances were measured by SSRM. SSRM requires that the material under investigation was deposited on a conductive substrate. The local surface potential was measured using KPFM. The SSRM and KPFM methods were two-pass techniques in which the first pass measured the topography and the second pass measured the electrical properties.

To identify potential insulation weak spots, an ED technique similar to those reported in the literature [13,19,20] was used. Patterned alumina wafers were placed in a  $\text{CuSO}_4$  electrolytic cell where the electrical contact was made with the rim of the wafer with the exposed Au surface. A current of 80 mA was applied for different time durations. The quality of the electrical insulation of the alumina film was evaluated with the potential of forming continuous copper film/channel in the regions with failing insulation spots under electrochemical deposition. A Zeiss optical microscope (OM) at low magnification was used to examine the surface of the wafer post electrodeposition.

Further studies of copper growth associated with insulation failures in the alumina were done using cross-sectional TEM (x-TEM). The regions with electrodeposited copper were cross sectioned through their apex to identify nucleation sites. Energy dispersive x-rays (EDX) technique was used to determine the composition of the electrodeposited copper and to identify the growth mechanisms.

## 3. Results and discussion

### 3.1. Thickness, structure and composition

TEM micrographs of the as deposited alumina films are shown in [Fig. 1](#). The Si surface was smooth, resulting in a clearly distinguishable alumina film. For clarity, the 2 and 4 nm  $\text{Al}_2\text{O}_3$  films have a protective platinum layer over the film surface. The 6 and 8 nm films have a protective carbon layer over the surface. These protective layers are required to safely prepare the samples by FIB. The FFT patterns of each alumina film displayed diffuse rings, dictating that they were amorphous in nature. (They are available in the [Supplementary information S.2](#).) While the TEM micrographs didn't identify any defects such as pinholes or pits, these defects may be present in the as-deposited films on the Si substrates. The TEM is capable of identifying defects down to the atomic level. However, if the number of defects were few, relatively small in size and largely dispersed, locating defects with TEM may not have been an optimal technique. Thus, other investigatory methods may be able to sense defects in the as-deposited films independent of the films' morphology.

The XPS high resolution data of the films deposited on Si and Au are shown in [Table 1](#). For alumina on Si, it was observed that the percentage of Al in the film increased with thickness whilst the percentage of O decreased. Disregarding carbon (C) in the spectra, the O:Al ratio decreased with the film thickness as shown in [Fig. 2](#). The target ratio of O:Al was 1.5. However, the contribution of a native  $\text{SiO}_2$  layer between the alumina and Si layers was expected to contribute to the O level in the ratio recorded by XPS. As the alumina deposited on Au would not contribute O from such an  $\text{SiO}_2$  layer, its XPS data was used to further

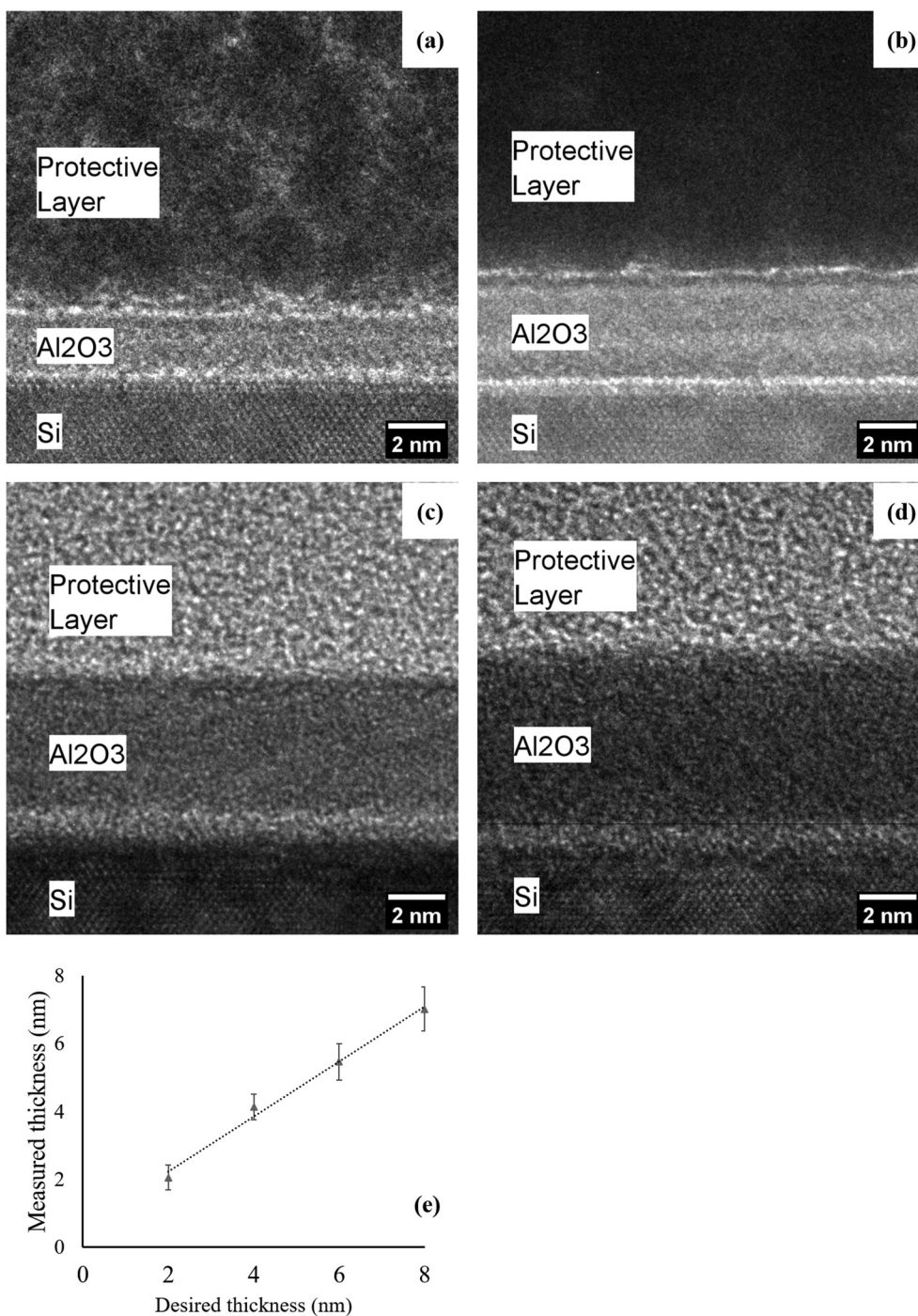


**Fig. 1.** (a–d) TEM scans of alumina on Si substrates. The bottom section of the scan is the  $\langle 1\ 0\ 0 \rangle$  Si substrates. (a) and (b) have protective platinum layers. (c) and (d) have protective carbon layers. (e) plot of measured thickness vs desired thickness of alumina film on Si substrates.

investigate the composition dependency on thickness. A similar trend was observed such that the relative percentage of O in the alumina decreases and relative percentage of Al increases as the overall thickness of the deposited alumina film increases. Thus, the relative O:Al ratio decreases with an increase of thickness. Interestingly, for the samples deposited on the Au substrate, the O:Al ratio is less than the nominal ratio of 1.5. Thus, these films have more Al and less O compared to the nominal ratio, whereas the films deposited on the Si substrate have less Al and more O compared to the nominal ratio. As the Al 2p signal exhibits peaks in a similar position to that of Au 4f, a scan using the Al 2s signal was also captured. While the ratios comparing O:Al using Al 2p and Al 2s vary with thickness, they exhibit the same

trend that the relative percentage of O decreases and the relative percentage of Al increases with thickness.

### 3.2. Surface state and nanoscale electrical properties

The measured roughness of alumina as a function of thickness slightly varied but did not exhibit an obvious thickness dependency. However, the measured roughness of the alumina did vary depending on the substrate. The roughness of the alumina on the Si is one order of magnitude less than that deposited on the Au. The difference is due to the Si wafer's surface being smooth per industry standards and the Au and TiW did not receive extra treatment to smoothen the surface prior

**Table 1**  
XPS high resolution spectra results for ultra-thin alumina deposited on Si.

Thickness (nm)	C 1 s (%)	Au 4f	O 1 s (%)	Al 2p/2s (%)	Rel O(%)	Rel Al (%)	O:Al
(Al 2p) 2	21.9	–	56.3	21.8	72	28	2.57
(Al 2p) 4	17.0	–	54.9	28.2	66.1	33.9	1.95
(Al 2p) 6	14.4	–	54.5	31.1	63.7	36.3	1.75
(Al 2p) 8	17.0	–	51.1	31.9	61.6	38.5	1.60
(Al 2p) 2	24.9	16.78	32.89	25.43	56.40	43.60	1.29
(Al 2p) 4	23.82	8.5	36.47	29.08	55.64	44.36	1.25
(Al 2p) 6	20.88	4	39.16	33.71	53.74	46.26	1.16
(Al 2s) 2	25.89	17.45	34.2	22.46	60.36	39.64	1.52
(Al 2s) 4	23.52	8.39	36.01	29.98	54.57	45.43	1.20
(Al 2s) 6	21.21	4.06	39.79	32.65	54.93	45.07	1.22

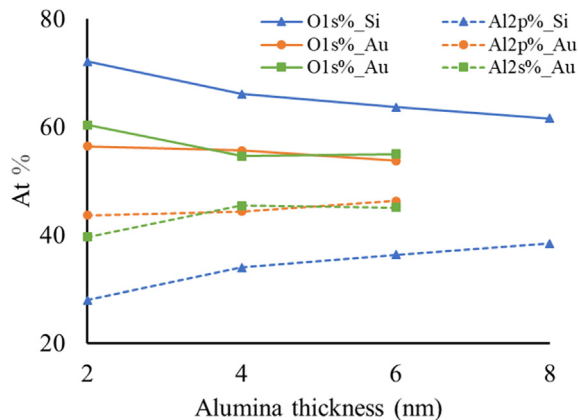


**Fig. 2.** Plot of Al and O relative percentages recorded by XPS. The atomic percentages vary as a function of thickness.

**Table 2**  
Roughness of alumina on Si and Au/TiW substrates.

Substrate/Roughness	Ra <sub>2</sub> (nm)	Ra <sub>4</sub> (nm)	Ra <sub>6</sub> (nm)	Ra <sub>8</sub> (nm)	Ra <sub>sub</sub> (nm)
Si	0.122	0.140	0.132	0.144	–
Au/TiW	2.335	2.49	3.043	–	2.719

to alumina deposition. Their difference is shown in Table 2. As the alumina deposited on the Si was quite smooth, any defects found on the surface were notable such as dust particles, whereas defects in the alumina deposited on the conductive surface were more difficult to distinguish due to the underlying topography.

The SSRM technique was performed on patterned alumina. The first scan measured the films topography and the second scan measured the current. To verify the suitability of the technique, the first scans were performed over the edge of the patterned alumina. The topography scan clearly identified the step height over the edge and the subsequent current profile showed that the alumina was insulating, and the Au surface was conductive as shown in Fig. 3. Large scans performed only over the alumina didn't show any conduction for 2, 4 and 6 nm films. This is interesting as a sharp change in the current response could be expected due to pinholes. It is possible that the size of the pinholes could be less than the radius of curvature of the scanning tip, which, as specified, by the manufacturer, is around 35 nm. As a result, the tip would pass over the pinhole and thus not register current through the pinhole. It is reported in the literature that conduction paths in ultra-thin insulators may form at grain boundaries [21], however, we didn't register currents in these areas.

The KPFM technique was performed on both the Si and the conductive substrates. The first scans measured topography and the second scan measured the surface potential. Similar to the method in SSRM, scans were performed over the edge of the patterned alumina on the

conductive surface. Again, the step height over the edge and the change in the surface potential due to an abrupt material change were visible in the plots. Interestingly, once the tip scanned only over the surface of the alumina, randomly dispersed changes in the surface potential were recorded. The changes in the surface potential did not appear to correlate with the topographical scan as no surface abnormalities were observed. The surface potential profiles contained several circular shaped regions where the potential reduced in magnitude. The surface potential fluctuation and its density varied with the alumina thickness as shown in Fig. 4 (a-f). The KPFM procedure was repeated for alumina deposited on the Si substrate. The surface potential measurements were similar to the alumina deposited on the conductive bilayer. Randomly dispersed variations of the surface potential were recorded across the film. Again, the density of this variation spread varied with the thickness of the alumina film as shown in Fig. 4 (g-l). KPFM measurements have highlighted abnormalities in the electrical state of the films regardless of the underlying substrate roughness. On the Si substrate, the density of potential variation decreased with increased thickness. However, on the Au/TiW surface, the variation does not show a clear trend dependent on film thickness. To understand the origin of this fluctuation further studies are required. The lack of any correlation between the surface potential and the corresponding topographical scans is interesting. If the surface potential and topographical scans were correlated there would have been a much clearer explanation that the defects had been morphological defects such as pinholes. On the other hand, electrical defects are never independent of the film structure regardless the surface topography. In particular, ultra-thin films are often amorphous or possess highly defective crystalline structures. The nature of these has a direct impact on the electronic density of states and electron transport.

### 3.3. Defect density and growth mechanisms

Due to the transparency and ultra-thin nature of the deposited films it was a significant challenge to identify the defect sites even using nanoscale investigation techniques. However, an ED method was able to identify the position of defect sites in the alumina film as copper grew at these sites on the surface of the film. The formation of these Cu growths was only possible due to voids or the electrical weak points being present in the alumina film. In agreement with the expectation, for the 2 nm alumina film, Cu was widely deposited over the surface, almost resembling a copper film, indicating that the insulation quality of the 2 nm film was very poor as shown in Fig. 5(a). The insulation quality was significantly improved as the film thickness increased from 4 to 8 nm. Fig. 5(b) shows that the insulation quality significantly improved for a 4 nm thick alumina film. Here, Cu is seen towards the rim of the wafer, where the plating contact was initially made and Cu was not visible at the centre of the wafer in contrast to the 2 nm alumina film. When the wafers were observed with an OM, it was observed that the electrodeposited Cu density decreased as the thickness of the alumina film increased. The improvement of insulation quality with alumina film thickness is shown in Fig. 5(c-e) for a 4, 6 and 8 nm film respectively. The growths were of higher density towards the north and south of the wafer and the density decreased towards the centre and towards the west and east. This was expected to be due to the sputtering conditions where the centre of the wafer was aligned with the centre of the target. While the growths indicate the presence of defect sites, they do not determine their nature or size. The size of the copper growth was dependent on the plating parameters (voltage, current, time, electrolyte concentration). For a thicker film, a longer plating time was required for the growths to form.

The size and the origin of these defects were further investigated using x-TEM. Samples were prepared by FIB with an attempt to cut through the apex of the Cu-growth assuming this to be the origin of the growth during the electrodeposition. Such preparations were carried out for films with alumina thickness of 4, 6 and 8 nm. Each of these

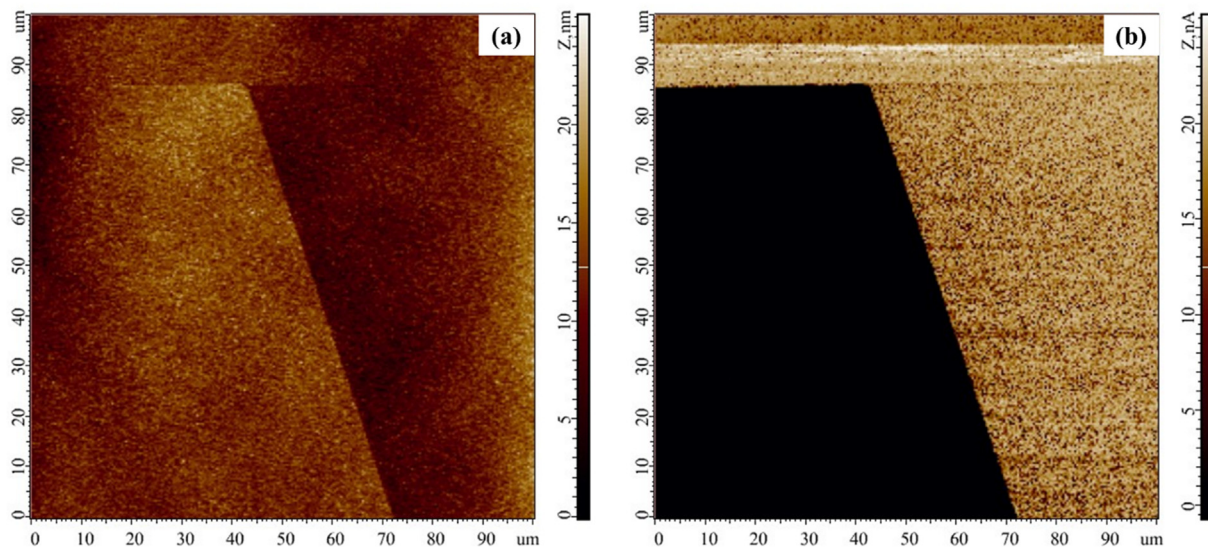


**Fig. 3.** Topographical (a) and current profile (b) scanned over a patterned 6 nm alumina film on the Au/TiW substrate. In (a) the step height over the edge was observed. In (b) the current profiles showed that the alumina is insulating and the Au/TiW substrate is conductive.

samples had different plating times and thus different sized growths. A typical x-TEM image is shown in Fig. 6 that shows the underlying Au/TiW/SiO<sub>2</sub> layers and a poorly resolved alumina layer at the Cu-Au interface. The size of the void and nucleation site for Cu was, however, difficult to distinguish.

EDX was employed to identify the nature of the nucleation sources. The scans were set to detect Al, Au, Cu, O, Si, Ti and W. The scans can clearly resolve the thicker layer such as the Si substrate, the thermally grown SiO<sub>2</sub> and the TiW and Au adhesion and conducting layers. The Cu island is also clearly distinguished. Due to the ultra-thin alumina film, the Al and O which compose the film are harder to distinguish but their presence is nonetheless, detected. For the 4 nm alumina film, Au was shown to diffuse outwards through the alumina into the Cu growth as shown in Fig. 7. For the Au to diffuse out from under the alumina layer, there must be an insulation weak point. This diffusion site is also located beneath the apex, suggesting that the growth initially formed at this point. It is likely that this occurred for the 6 and 8 nm film but we could not confirm as our attempts of FIB cross-sectioning in these films, even after several attempts, could not take place in a region proximal to the apex. It may also be possible that FIB had cut directly through this area in the cutting process.

### 3.4. Correlation between growths, surface charge and composition

The ED method clearly highlighted that there are widely dispersed weak points in the alumina film that would be impractical to locate with EM and traditional scanning probe methods. The density of the defect points has been identified to be dependent on the film thickness and the position on the wafer. While AFM didn't register any clear alumina surface abnormalities, use of KPFM identified fluctuations in the electrical state of the alumina regardless of the substrate type. When the alumina film was thinner, there was a high density of sites where the surface potential of the film fluctuated. When the alumina film thickness was increased, the density of sites where the alumina surface potential varied decreased. The surface potential deviation has a possible correlation with the O:Al ratio as recorded by XPS. For both substrates, the O:Al ratio decreased as the film thickness increased. The changes are speculated to be due to a change in the number of Al and O vacancies in the film, affecting the structure and thus the density of states and charge transport. These defects were expected to have enabled the growth of Cu on the surface of the alumina from a nucleation site on the Au underlayer.

## 4. Conclusions

From an industrial perspective, sputter deposition of insulating films is beneficial for relatively thin films where low cost and high throughput are required. However, depositing films with uniform thickness and electrical properties under 10 nm is a challenge. Thinner films are likely to have increased numbers of defects compromising the functionality of the film for its target application. Many studies on such films are often performed on relatively small substrates up to 4 × 4 cm<sup>2</sup>, therefore not entirely replicable on larger industrial sized substrates. We have performed several experimental methodologies and characterisation techniques to identify defects in ultra-thin insulators deposited by RF magnetron sputtering on substrates 200 mm in diameter.

TEM is a proven and established technique used in the investigation of nanometric properties. However, here, due to the transparency of ultra-thin alumina and the relatively widely dispersed nature of these defects, it is an impractical technique to locate such defects, unless their precise location is known. If there are pinholes or pits in the alumina film, a combination of AFM and SSRM would have expected to record this as a dip in the surface coinciding with a spike in current. However, this was not observed in the case with our alumina films deposited on a conductive substrate.

Variations in the electrical state of the alumina films were observed using KPFM. It is of significant interest that the corresponding topographical scans didn't identify any surface abnormalities. These results suggest that while the surface may not appear defective from a topographical viewpoint, there may be charge abnormalities on the surface or in isolated areas beneath the surface of the alumina. The surface potential fluctuations tended to decrease as the thickness of the film increased.

An electrodeposition technique clearly identified leakage spots in the alumina as Cu islands grew on the surface. For Cu to grow, there needs to be a path for Cu to impinge to the surface or Au seed layer to diffuse. We observed that the electrical insulation quality of sputter deposited alumina films increased with the film thickness. Again, if there was a direct pinhole, it is speculated that these defects would have been recorded by SSRM and AFM. However, KPFM indicates their maybe weak points in the film which may allow charge carrier motion and thus promote growth of Cu islands on the surface of the alumina.

As the film thickness increased, the Al content increased as recorded by XPS of alumina deposited on the Si and Au substrate. The non-

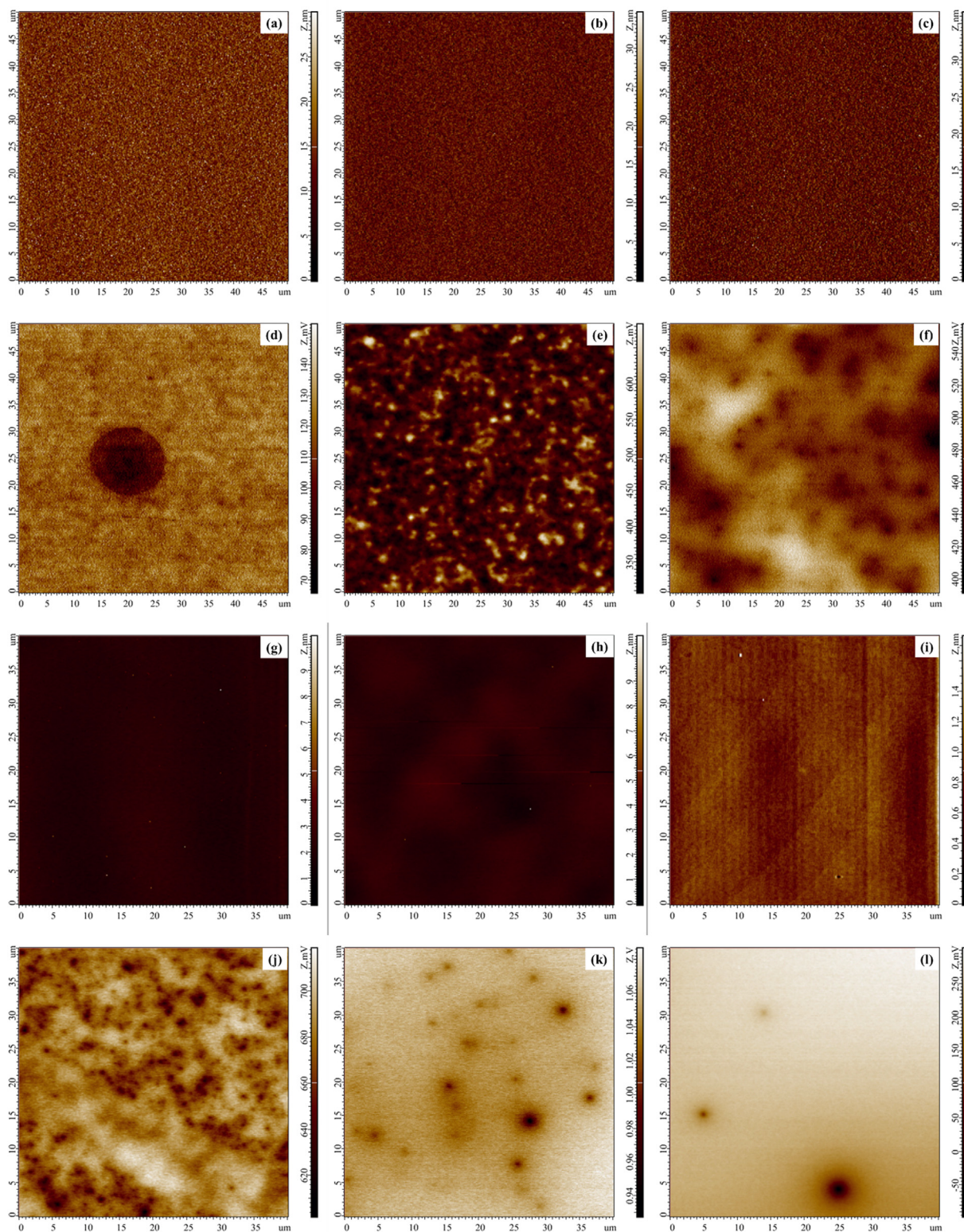


**Fig. 4.** (a – c) 50 μm × 50 μm topographical scans of 2, 4 and 6 nm of alumina on the Au/TiW surfaces respectively and in (d – f) their corresponding surface potential scans. In (g – i) 40 × 40 μm topographical scans of 2, 4 and 6 nm of alumina on the Si surfaces respectively and in (j – l) their corresponding surface potential scans.

stoichiometric nature of the deposited film is expected to cause structural defects causing a charge imbalance or contribute to vacancies. The presence of charge imbalances instead of pinhole formation may explain why AFM and SSRM were not able to detect any pinholes or record any current spikes. While also partially explaining why the AFM

and KPFM profiles did not correlate.

CMOS, MEMS and NEMS devices fabricated on an industrial scale may use nanoscale films that are deposited on relatively large substrates up to and beyond 200 mm in diameter. If these nanoscale films also possess nanometric and dispersed defects, certain nanoscale techniques

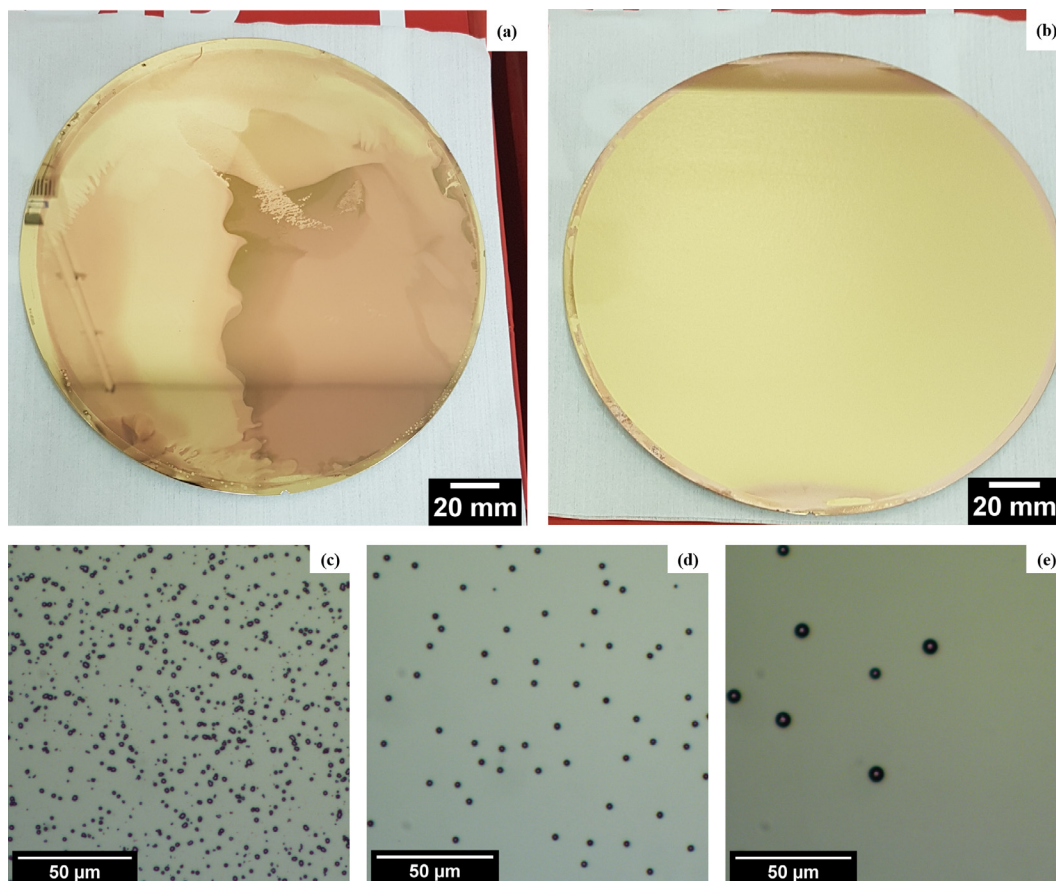


Fig. 5. 200 mm diameter wafers used for electrodeposition. (a) was a 2 nm film where Cu formed across the wafer. (b) was a 4 nm film, where Cu is observed on the wafer rim where the probes made contact. The bright surface is the Au layer under the alumina. (c-e) shows randomly dispersed Cu growths in the shape of circular dots on the surface of 4, 6 and 8 nm alumina films. The density of growths were dependent on the thickness of the alumina film and their position on the wafer.

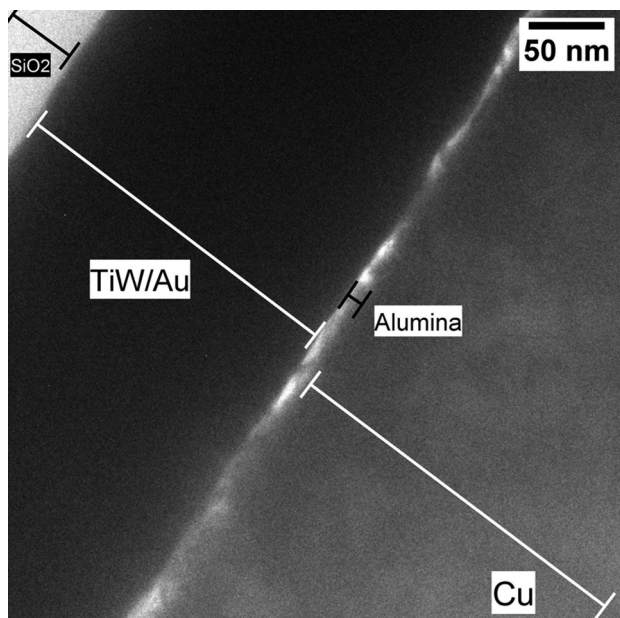


Fig. 6. x-TEM through the apex of a Cu growth on an 8 nm alumina film. From the top left corner to the bottom right corner, the scan displayed SiO<sub>2</sub>, TiW/Au, alumina and Cu. Variations in intensity of the alumina layer are defect sites that are expected to contribute to the Cu formation.

may not be practical for investigation due to the large substrate size. This is particularly important if the defects are independent of the

topography of the films. Our suggested combination of electrodeposition and KPFM techniques were able to localise and identify electrical weak spots in ultra-thin alumina on 200 mm diameter substrates that would be impractical and challenging to identify with traditional OM, SEM, TEM and AFM.

Our methodology has provided a basis to optimise the deposition parameters for RF magnetron sputtering of ultra-thin alumina on large industrial scale substrates. The results will aid in the improvement of the quality and functionality of ultra-thin alumina deposited on 200 mm diameter substrates used in the fabrication of CMOS, MEMS and NEMS devices.

**Declaration of Competing Interest**

The authors declare that they have no known competing financial interests or personal relationships that could have appeared to influence the work reported in this paper.

**Acknowledgements**

The authors would like to acknowledge the funding contributed by the Irish Research Council’s Enterprise Partnership Scheme under the project ID: EBPPG/2016/271 and by Analog Devices, Inc. The FEG-TEM used was funded by the Higher Education Authority (HEA), Ireland under its Program for Research in Third Level Institute (PRTL) cycle 4. The NTEGRA-Spectra Hybrid Nanoscope was funded by Science Foundation Ireland (SFI) Opportunistic Fund for research infrastructure. The Dual Beam Focussed Ion Beam and X-ray Photoelectron Spectrometer have been funded by SFI Research Infrastructure

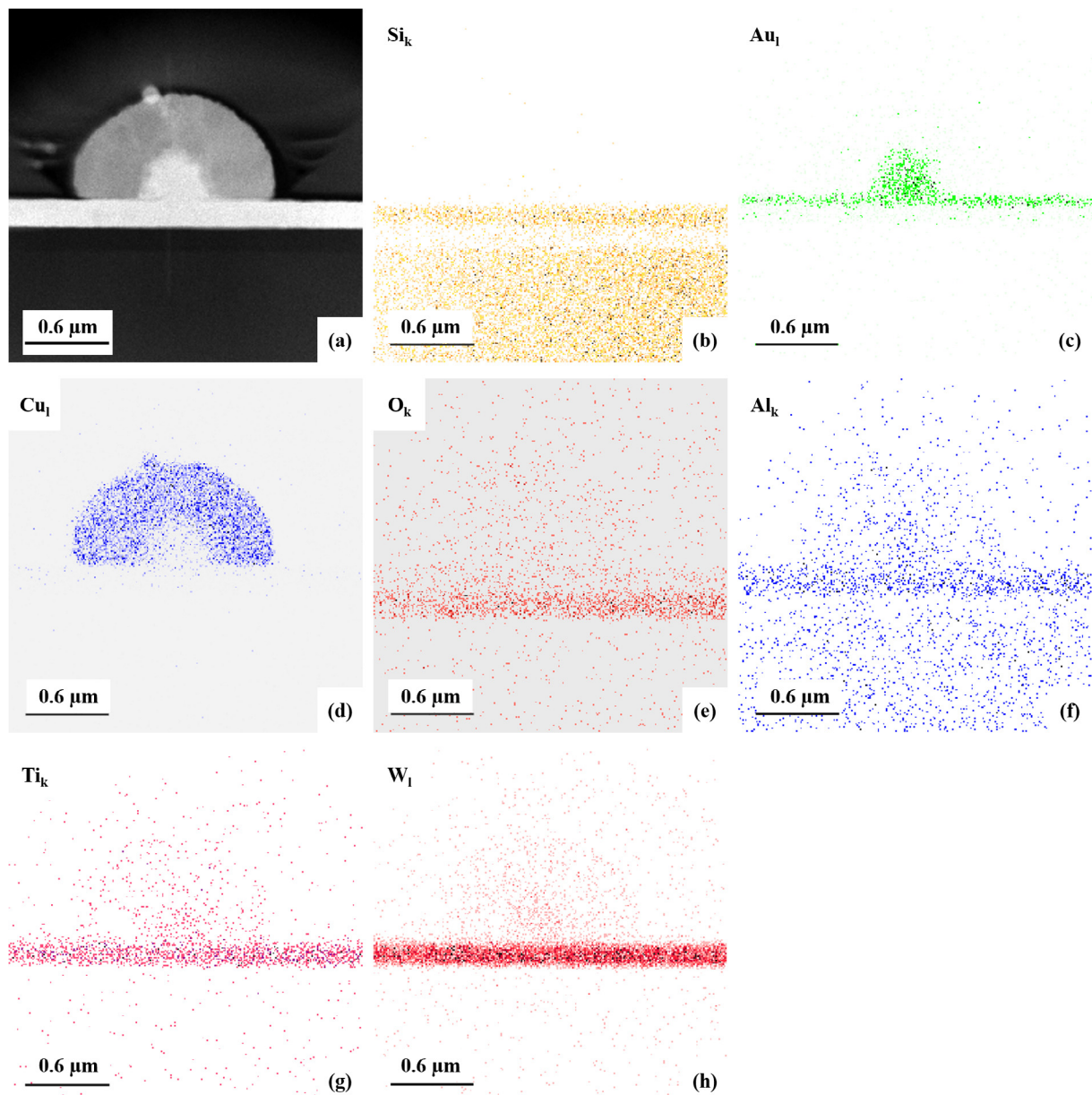


Fig. 7. EDX composition map of Cu growth on 4 nm alumina. (a) STEM scan area, (b)  $\text{Si}_k$ , (c)  $\text{Au}_l$ , (d)  $\text{Cu}_l$ , (e)  $\text{O}_k$ , (f)  $\text{Al}_k$ , (g)  $\text{Ti}_k$ , (h)  $\text{W}_l$ . EDX indicates that Au diffused outwards through the alumina layer during electrodeposition.

programme.

## Appendix A. Supplementary data

Supplementary data to this article can be found online at <https://doi.org/10.1016/j.apsusc.2020.146950>.

## References

- [1] G. Balakrishnan, et al., Effect of substrate temperature on microstructure and optical properties of nanocrystalline alumina thin films, *Ceram. Int.* 39 (8) (2013) 9017–9023.
- [2] I.N. Reddy, et al., Pulsed rf magnetron sputtered alumina thin films, *Ceram. Int.* 40 (7) (2014) 9571–9582.
- [3] B.V. Hanby, B.W. Stuart, M. Gimeno-Fabra, J. Moffat, C. Gerada, D.M. Grant, Layered  $\text{Al}_2\text{O}_3\text{-SiO}_2$  and  $\text{Al}_2\text{O}_3\text{-Ta}_2\text{O}_5$  thin-film composites for high dielectric strength, deposited by pulsed direct current and radio frequency magnetron sputtering, *Appl. Surf. Sci.* (2019).
- [4] R. Khosla, E.G. Rolseth, P. Kumar, S.S. Vadakupudhupalayam, S.K. Sharma, J. Schulze, Charge trapping analysis of metal/ $\text{Al}_2\text{O}_3/\text{SiO}_2/\text{Si}$ , gate stack for emerging embedded memories, *IEEE Trans. Device Mater. Reliab.* 17 (1) (2017) 80–89.
- [5] I. Neelakanta Reddy, V. Rajagopal Reddy, N. Sridhara, S. Basavaraja, A.K. Sharma, A. Dey, Optical and microstructural characterisations of pulsed rf magnetron sputtered alumina thin film, *J. Mater. Sci. Technol.* 29 (10) (2013) 929–936, <https://doi.org/10.1016/j.jmst.2013.05.002>.
- [6] S. Chen, L. Tao, L. Zeng, R. Hong, RF magnetron sputtering aluminum oxide film for surface passivation on crystalline silicon wafers, *Int. J. Photoenergy* 2013 (2013).
- [7] C.-Y. Lee, et al., Evaluating the impact of thermal annealing on c-Si/ $\text{Al}_2\text{O}_3$  interface: Correlating electronic properties to infrared absorption, *AIP Adv.* 8 (7) (2018) 075204.
- [8] M. Serényi, T. Lohner, G. Sáfrán, J. Szívós, Comparison in formation, optical properties and applicability of DC magnetron and RF sputtered aluminum oxide films, *Vacuum* 128 (2016) 213–218, <https://doi.org/10.1016/j.vacuum.2016.03.033>.
- [9] R. Boidin, T. Halenkovič, V. Nazabal, L. Beneš, P. Němec, Pulsed laser deposited alumina thin films, *Ceram. Int.* 42 (1) (2016) 1177–1182.
- [10] P. S. M. R. G. J. S. K. M. D. and G. V., “Dielectric properties of DC reactive magnetron sputtered  $\text{Al}_2\text{O}_3$  thin films,” *Thin Solid Films*, vol. 520, no. 7, pp. 2689–2694, 2012/01/31/ 2012, doi: <https://doi.org/10.1016/j.tsf.2011.11.040>.
- [11] T.-T.A. Li, et al., Influence of oxygen on the sputtering of aluminum oxide for the surface passivation of crystalline silicon, *Sol. Energy Mater. Sol. Cells* 95 (1) (2011) 69–72.
- [12] S. Prasanna, et al., Composition, structure and electrical properties of DC reactive

- magnetron sputtered Al<sub>2</sub>O<sub>3</sub> thin films, *Mater. Sci. Semiconduct. Process.* 16 (3) (2013) 705–711, <https://doi.org/10.1016/j.mssp.2012.12.012>.
- [13] Y. Zhang, et al., Investigation of the defect density in ultra-thin Al<sub>2</sub>O<sub>3</sub> films grown using atomic layer deposition, *Surf. Coat. Technol.* 205 (10) (2011) 3334–3339.
- [14] J. Acharya, J. Wilt, B. Liu, J. Wu, Probing the dielectric properties of ultrathin Al/Al<sub>2</sub>O<sub>3</sub>/Al trilayers fabricated using in situ sputtering and atomic layer deposition, *ACS Appl. Mater. Interfaces* 10 (3) (2018) 3112–3120.
- [15] X. Tang, Z. Li, H. Liao, J. Zhang, Growth of ultrathin Al<sub>2</sub>O<sub>3</sub> films on n-InP substrates as insulating layers by RF magnetron sputtering and study on the optical and dielectric properties, *Coatings* 9 (5) (2019) 341.
- [16] J. Kohout, et al., Stable reactive deposition of amorphous Al<sub>2</sub>O<sub>3</sub> films with low residual stress and enhanced toughness using pulsed dc magnetron sputtering with very low duty cycle, *Vacuum* 124 (2016) 96–100, <https://doi.org/10.1016/j.vacuum.2015.11.017>.
- [17] J. Lin, High rate reactive sputtering of Al<sub>2</sub>O<sub>3</sub> coatings by HiPIMS, *Surf. Coat. Technol.* 357 (2019) 402–411.
- [18] U. Kashniyal, K.P. Pandey, Stress induced degradation and reliability of Al<sub>2</sub>O<sub>3</sub> thin film on silicon, *Vacuum* 152 (2018) 109–113.
- [19] Y. Zhang, J.A. Bertrand, R. Yang, S.M. George, Y. Lee, Electroplating to visualize defects in Al<sub>2</sub>O<sub>3</sub> thin films grown using atomic layer deposition, *Thin Solid Films* 517 (11) (2009) 3269–3272.
- [20] K. Chu, et al., Quantitative analysis of nano-defects in thin film encapsulation layer by Cu electrodeposition, *Appl. Surf. Sci.* 453 (2018) 31–36.
- [21] W. Lu, L.-M. Wong, S. Wang, K. Zeng, Local phenomena at grain boundaries: An alternative approach to grasp the role of oxygen vacancies in metallization of VO<sub>2</sub>, *J. Materomics* 4 (4) (2018) 360–367.